Rutherford Scattering

Edward Jin
MIT Department of Physics
(Dated: April 14, 2022)

By scattering α particles produced by ^{241}Am on gold foil, the scattering-cross section per atom of gold leading to deflections above $\theta = (2.6 \pm 0.3)^\circ$ was measured to be $(4.0 \pm 0.4) \times 10^{-24}\,\mathrm{m}^2$. In addition, by varying the scattering angle, thickness, and type of the target, the Rutherford differential cross section formula for the nuclear atom was verified, in terms of angular dependence, atomic number dependence, and energy dependence, all within 2σ. Finally, by measuring the change in particle energy, the thickness of the gold foil itself was measured to be $(1.96 \pm 0.06)\,\mu\mathrm{m}$.

I. INTRODUCTION

In the early 1900s, scientists began investigating the structure of the atom. One of the first models of the atom, named the 'plum pudding' model, envisioned an atom as a sphere of positive charge, with electrons being distributed across the sphere. Unfortunately, this model failed to explain the numerical regularities of optical emission wavelengths found by Balmer.

Another piece of experimental evidence against this model was with scattering experiments, carried out by Rutherford. In these experiments, charged α particles produced by radioactive decay are sent through metal foils, and their angular deflection θ is measured. With the plum pudding model, the α particle would experience many random small-angle deflections as they traverse the foil, leading to extremely low probability of large scattering. Specifically, Rutherford showed that the fraction of particles scattered at an angle $\geq \theta$ was given by

$$f(\theta) \approx \exp(-\theta^2/\theta_m^2)$$

where θ_m^2 is the *mean multiple scattering angle*, equal to about 1° for gold foil. The sharp peak of this function meant that under the plum pudding model, large-angle scattering was essentially impossible [1].

However, Rutherford found that large-angle scattering did indeed happen at an observable rate, thus disproving the plum pudding model. By instead modeling the atom with a small nucleus that concentrated positive charge, and modeling the trajectories of alpha particles near the nuclei, he derived the *Rutherford scattering differential cross section per target atom*:

$$\frac{d\sigma}{d\Omega} = \left(k_e \frac{ZZ'e^2}{4E}\right)^2 \cdot \frac{1}{\sin^4(\theta/2)}$$

where θ is the scattering angle, k_e is the electrostatic constant, Z and Z' are the atomic numbers of the incident particle and target, and E is the kinetic energy of the incident particle [1].

The number of particles scattered at a specific angle is then given by $I_0 N \frac{d\sigma}{d\Omega} \cdot \Delta\Omega$, where I_0 is the incident particle flux, N is the area density of the target, and $\Delta\Omega$ is the solid angle that the detector subtends [2]. The area density is given by $N = \frac{\rho_Z t_Z N_a}{M_Z}$ where N_a is Avogadro's number, M_Z is the atomic mass of Z, and ρ_Z is the density of Z.

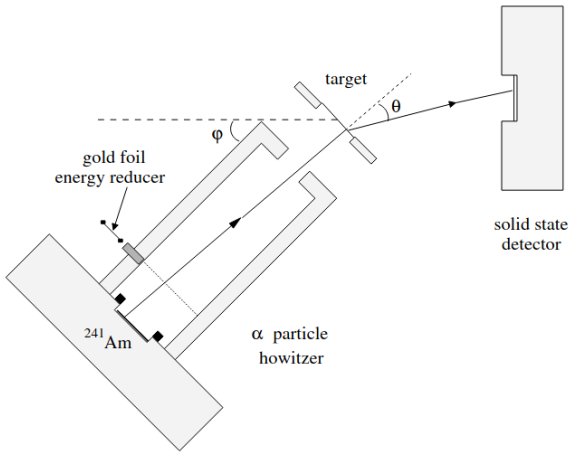

FIG. 1. A diagram of the experimental setup. α particles produced by ^{241}Am first pass through a gold-foil energy reducer, and then hit the target itself, before scattering at an angle of θ into the detector. The howitzer itself can be rotated, in order to measure various scattering angles. Adapted from [1].

Thus, keeping the detector setup constant, we have:

$$\text{Rate} \propto \frac{Z^2 \rho_Z t_Z}{M_Z} \cdot \frac{1}{E^2} \cdot \frac{1}{\sin^4(\theta/2)}.$$

We can then verify these proportionalities by varying the target foil and scattering angle θ.

II. EXPERIMENTAL SETUP

A $1.5\,\mathrm{mCi} \cdot \mathrm{in}^{-2}$ activity ^{241}Am α-particle source (5.5 MeV), which is sealed with a protective evaporated gold coating of $1.5\,\mu\mathrm{m}$ thickness, is positioned inside a howitzer of length 8 cm and radius 0.25 in. The howitzer is pointed directly at a target with radius 0.5 in, whose center is 14 cm away from a silicon barrier detector of radius 0.5 in. The howitzer and target is rotationally adjustable and can be rotated all the way around the chamber, in order to observe various scattering angles.

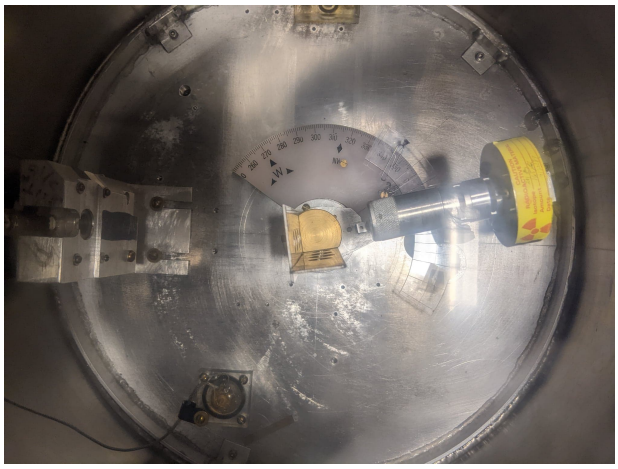

FIG. 2. A run at a $\theta = 14.4^\circ$ scattering angle. The howitzer on the right is positioned to be in line with the gold foil target, and counts are recorded by the silicon barrier detector on the left.

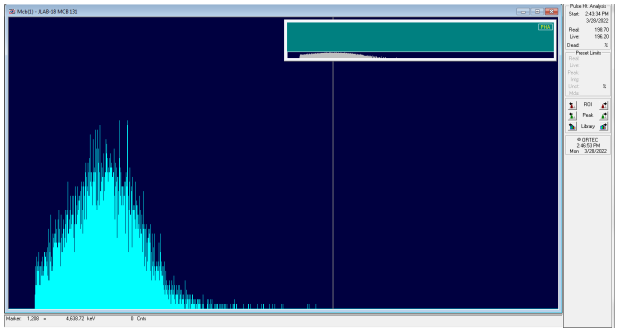

FIG. 3. A sample MCA output. This measurement is obtained by scattering through an iron foil at 0°.

The silicon barrier detector is connected to a Canberra 2006 pre-amplifier, which converts the detector signal to a step voltage pulse proportional to the total charge. This signal is then amplified again with a Canberra 471 Spectroscopy Amplifier, set to a gain of 500, to produce output pulses of approximately 7 V. These pulses get passed into an Ortec Multi-Channel Analyzer, which records all pulses and sorts them by energy.

III. EXPERIMENTAL PROCEDURE

III.1. General Measurement Procedure

Vacuum was applied to the entire chamber until the pressure reading was below 200 microns of mercury. Then, the target was set in place and the howitzer (along with the target) were rotated to the desired angle. The exact angle between the howitzer and the detector was recorded with a phone camera placed at a constant position. The chamber was then covered to prevent ambient light from reaching the detector, and the experiment was run until clear peaks could be seen in the MCA readings. In practice, this meant a few minutes for high-intensity peaks, and a few days for low-intensity peaks.

III.2. General Peak-Finding Procedure

To find peak locations, we fit a Gaussian to the peak produced by the MCA. The peaks themselves had longer tails on the left than what would be expected from a Gaussian. However, by including only data points near the center of the peaks, Gaussian distributions fit well, as tested by χ^2 tests. Thus, to find peak position, we first fit a rough Gaussian to the whole dataset (after removing background noise). Afterwards, we used that estimate of the mean and standard deviation to include only the data within 2σ of the mean, and finally fitted those datapoints to determine the peak's center location.

In order to estimate the systematic uncertainty of the fitting procedure, we fit the peak multiple times, using data from within $1\sigma, 1.5\sigma, 2\sigma, 2.5\sigma$, and 3σ of the mean. We then took the maximum difference between fitted peak locations as the systematic uncertainty for this peak-finding procedure.

IV. EXPERIMENTS AND RESULTS

IV.1. Energy Calibrations

The variation of stopping power with respect to kinetic energy is known from the NIST database on α-particle stopping energies [3]. Using a piecewise linear interpolation for stopping power and numeric integration, we can then predict the particle energy after traversing a specific distance.

By using the known thickness of $(1.50 \pm 0.05)\,\mu\text{m}$ for the deposited gold foil on the howitzer, and using the major peak of the initial ^{241}Am decay energy of 5.486 MeV, we find that the energy of the incident open-hole radiation should be $(4.833 \pm 0.023)\,\text{MeV}$. Using an open-hole energy measurement (see Sec. IV.2) as a baseline for the correspondence between channel number and energy, we obtain a ratio of $(3.389 \pm 0.024)\,\text{keV}$ per channel number. This correspondence between channel number and energy is used for all future energetic measurements.

IV.2. Gold Foil Thickness

By varying the number of the gold foils in the target, we observed marked changes in the resulting energies of the α particles on the MCA. Using the peak-fitting procedure and stopping power integration, we respectively obtain the final energies and corresponding thicknesses of the gold foils. A linear fit between the number of foils and the final energies was reasonable, with a χ^2 value of 3.0 with corresponding probability

$P(\chi^2 > 3.0; df = 2) = 22\%$. The exact results are tabulated below:

Sample	Energy	Thickness per Foil
Open Hole	(4833 ± 33) keV	NA
1 Gold Foil	(3824 ± 38) keV	(2.09 ± 0.15) µm
2 Gold Foils	(2903 ± 27) keV	(1.90 ± 0.06) µm
3 Gold Foils	(1738 ± 68) keV	(1.88 ± 0.06) µm
Average	NA	(1.96 ± 0.06) µm

IV.3. Scattering Cross-Section

To estimate the overall scattering cross section, we looked at the rate of scattering by computing the difference of rates between the open hole and gold foil target at $\theta = 0°$. A 0.49 ± 0.01 fraction of particles are scattered by the gold foil beyond the detector. Since the ratio should also be given by $N \cdot \sigma$, where N is the number density per area, we can calculate the cross-section $\sigma = (4.0 \pm 0.4) \times 10^{-24}\,\mathrm{m}^2$.

We also note that a scattering angle $\theta = 2.6° \pm 0.3°$, corresponding to the detector width, has impact parameter $b = (1.05 \pm 0.13) \times 10^{-12}\,\mathrm{m}$. The circular scattering cross section then has area $(3.5 \pm 0.7) \times 10^{-24}\,\mathrm{m}^2$. This theoretical estimate is in line with the experimental estimate based on scattering rates.

IV.4. Angular Distribution

As the detector has nonzero angular acceptance, particles can actually scatter through a range of angles while still hitting the detector. In order to obtain an accurate model of the cross section's angular dependence, we measure the spread of the howitzer's angular distribution.

Let the angular response function $g(\theta, \phi)$ be the probability density function (with respect to θ) of scattering an angle θ, when the howitzer is at an angle ϕ. Then, the recorded count rate at an angle ϕ is

$$f(\phi) = \int_{\theta_0}^{\pi} g(\theta, \phi) r(\theta)\, d\theta$$

where $r(\theta) \propto \sin^{-4}(\theta/2)$ is the count rate of scattering at an angle of θ, and θ_0 is a physically-imposed cutoff angle. We can measure the angular distribution $h(\theta)$ by observing the count rates through an open hole at small angles, and then set $g(\theta, \phi) = h(\theta - \phi)$ to be the angular response at an arbitrary howitzer angle ϕ.

To measure $h(\theta)$, the howitzer and an open hole target were rotated to angles between $-8°$ and $8°$, at approximately $2°$ degree angles. Counts were recorded for only a few minutes, as the count rates at small angles are high. The resulting count rates, along with a fitted Gaussian, are displayed in Fig 4. The y-uncertainties were calculated by assuming a $\pm 0.1°$ uncertainty in the angle, and by measuring the variation of the fitted count rate when the input angle is shifted by such an amount.

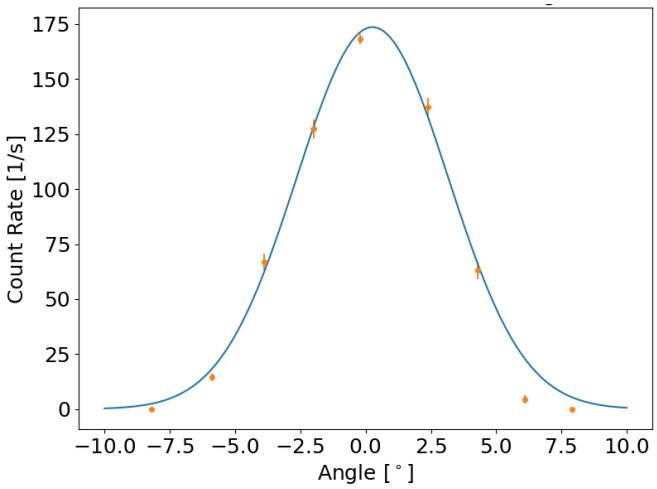

FIG. 4. The variation of count rate as a function of howitzer position. The Gaussian fit, taking into account only the 5 central data points, has a χ^2 value of 5.64, with corresponding probability $P(\chi^2 > 5.64; df = 2) = 6\%$.

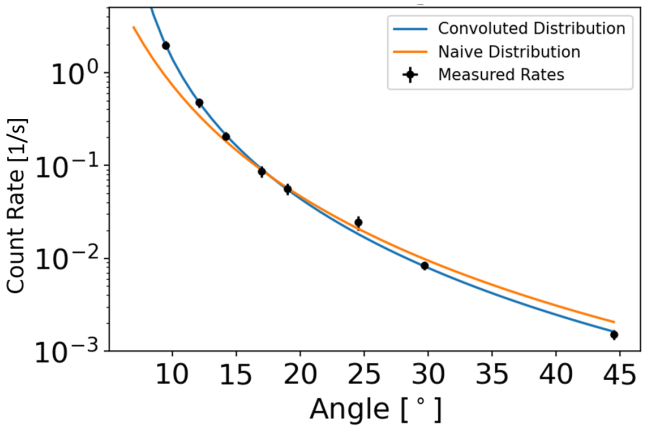

FIG. 5. The count rates as a function of scattering angle. The naive distribution represents the direct fit of the $\sin^{-4}(\theta/2)$ dependence, and has a χ^2 value of 46.40 with $P(\chi^2 > 46.40; df = 7) \approx 0$. The distribution resulting from the convolution of the Gaussian angular response and $\sin^{-4}(\theta/2)$ performs much better, with a χ^2 value of 5.03 and corresponding probability $P(\chi^2 > 5.03; df = 6) = 54\%$.

Although the Gaussian fit for the angular distribution overestimates the count rate at the tails of the distribution, it interpolates the center of the peak well. Since the majority of the counts come from the center of the peak, the small additive errors in the tails only introduce small uncertainties in the resulting count rate.

IV.5. Angular Dependence of Scattering

The howitzer and target were rotated to various angles, ranging from $\approx 10°$ to $\approx 45°$, and the thinnest gold foil was chosen as the target. The count rate through the

gold foil at each angle was then measured, for a time sufficient to obtain hundreds of counts. Due to the presence of background radiation, only counts from channels 861 to 1374 (encompassing nearly the entirety of the previously-measured 0°-scattering gold peak) were used in the rate measurement. In order to estimate the systematic uncertainty of this cut, we note that even after extending the window by 250 counts in both directions, only at most a 11% deviation in the rate was observed in the case of large-angle scattering. By plotting the rates in Fig. 5, we observe the $\sin^{-4}(\theta/2)$-dependence as predicted by Rutherford's formula, after convoluting with the angular response function derived above.

IV.6. Energetic Dependence of Scattering

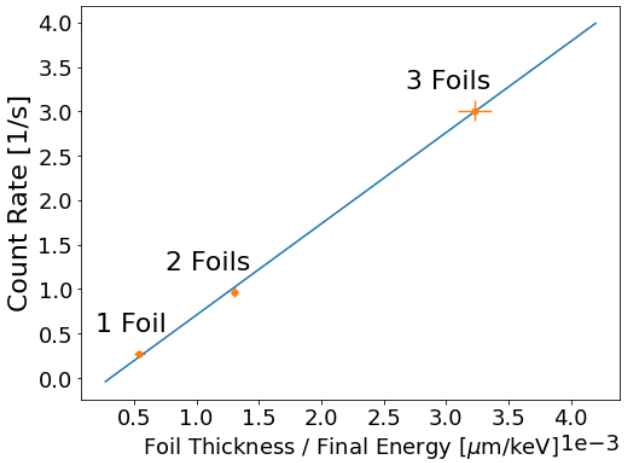

FIG. 6. The relation between energy and count rate. The linear fit has a $\chi^2 = 0.8$ with corresponding probability $P(\chi^2 > 0.8; df = 1) = 38\%$.

The Rutherford differential cross-section formula also includes an energy dependence. Since the energy of the particle varies as it goes through the foil, we should instead use the average value $\langle \frac{1}{E^2} \rangle \approx \frac{1}{E_{final} E_{initial}}$ in the formula. Thus, the rate of scattering should be directly proportional to thickness divided by final energy.

To verify this relationship, we scattered off of various numbers of gold foils at $\theta = 15°$, and measured the corresponding count rates, by counting the total number of events, and then subtracting off the background rate. Combining this rate data with the thickness and energetic data from the previous section, we obtain the plot in Fig. 6, and verify the formula's energy-dependence.

IV.7. Z-dependence of the Rutherford cross-section

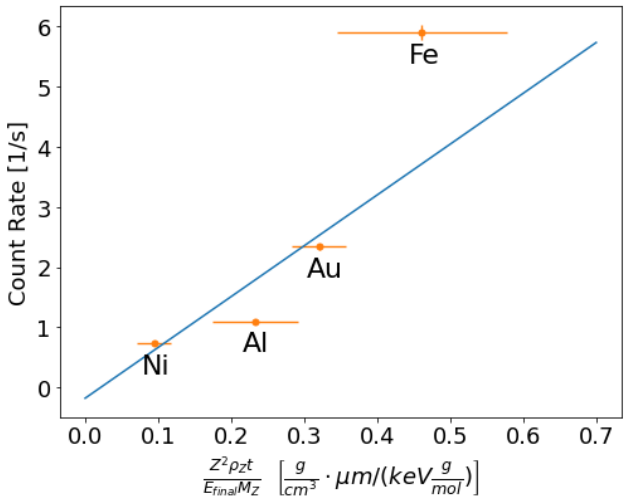

FIG. 7. The relationship of Z to count rate. The uncertainties in x are very large, due to the 25% stated uncertainty in thicknesses. The gold data used the thickness calculated previously, taking into account new uncertainties from the fact that the measurements were not done with exactly the same angle. The linear fit has a $\chi^2 = 6.3$ with corresponding probability $P(\chi^2 > 6.3; df = 2) = 5\%$.

The Rutherford differential cross-section formula further includes a quadratic dependence on atomic number. To investigate this relationship, we scattered off of various metals with known thickness at $\theta = 10°$, in addition to the 10° gold data collected earlier. Each element has a different thickness, density, final energy, and atomic mass; taking all of these into account, the count rate should be proportional to $\frac{Z^2 \rho_Z t}{E_{final} M_Z}$. Plotting this quantity against rate shows agreement (Fig. 7) within 2σ.

V. CONCLUSION

In this experiment, we used ^{241}Am α particles to perform scattering experiments on various target foils and measure the cross-section of gold to be $(4.0 \pm 0.4) \times 10^{-24}\,\mathrm{m}^2$. By varying the angle of scattering and type of target, we successfully verify the nuclear atom model's theoretical dependence on angle, energy, and nuclear charge within 2σ. In addition, we show that energy loss data can be used to measure foil thicknesses, by measuring the thickness of a gold foil to 3% uncertainty.

[1] MIT Department of Physics, "Rutherford Scattering," http://web.mit.edu/8.13/www/JLExperiments/JLExp15.pdf.
[2] A. Melissinos and J. Napolitano, "Experiments in modern physics," (Academic Press, 1966) 1st ed.
[3] NIST, "ASTAR Database," https://physics.nist.gov/PhysRefData/Star/Text/ASTAR.html.